Spectral Matching Techniques to Determine Historical Land-use/Land-cover (LULC) and Irrigated Areas Using Time-series 0.1-degree AVHRR Pathfinder Datasets

P.S. Thenkabail, P. GangadharaRao, T.W. Biggs, M. Krishna, and H. Turral

Abstract

*This study established spectral matching techniques (SMTs) to determine land-use and land-cover (LULC) and irrigated area classes from historical time-series (HTS-LULC) AVHRR 0.1-degree pathfinder satellite sensor data. The approach for HTS-LULC mapping and characterization was to develop "target" spectra from: (a) Recent Time Series for which LULC and irrigated area classes (RTS-LULC) were mapped using extensive ground-truth data, and (b) ideal locations, which are known endmembers even during historical time-periods of interest, as determined based on existing knowledge base including agricultural census data. The HTS-LULC for the period of 1982 to 1985 and RTS-LULC for the period of 1996 to 1999 were established using monthly continuous time-series AVHRR mega-file data of 192 bands (48 months * 4 AVHRR bands per month) each for the HTS and RTS time periods. The study was conducted in the Krishna river basin (India), which has a large area (267,088 km^2) with numerous irrigation projects and high population density.*

The quantitative and qualitative SMTs were used to identify and label HTS LULC classes. The identification and labeling process begins with qualitative spectral matching technique which visually matches the time-series NDVI spectra of known RTS-LULC classes and/or ideal endmember classes with time-series spectra of HTS-LULC classes. This helps identify classes of similar spectral characteristics in terms of shape and magnitude over time. The quantitative SMTs involved: (a) spectral correlation similarity (SCS), as a shape measure, (b) Euclidian distance (E_d), as distance measure, (c) spectral similarity value (SSV) as a combination of shape and distance measure, and (d) modified spectral angle similarity (MSAS) as a hyperangle measure. The quantitative and qualitative SMT methods and techniques lead to assigning HTS-LULC classes that match RTS-LULC names. In all, an aggregated seven HTS-LULC that were spectrally similar to the seven RTS-LULC classes and/or ideal endmember classes were identified and labeled. The SSV was the best method, followed by SCS.

The validity of SMTs in identifying HTS LULC classes were determined based on calculations of irrigated areas. The 1982 to 1985 HTS irrigated area was 2,975,800 hectares which was 8.5 percent higher than the non-remote sensing based irrigated area estimate for 1984 (2,743,638 hectares) by India's Central Board of Irrigation and Power (CBIP). The results show that the irrigated areas in Krishna basin increased by 29.7 percent in 1996 to 1999 (3,860,500 hectares) relative to 1982 to 1985 (2,975,800 hectares), mostly concentrated in the northwestern portion of the basin. The results clearly imply the strengths of the spectral matching techniques in identifying and labeling LULC and irrigated area classes from the historical satellite sensor data for which little or no ground truth data is available.

Introduction

Well calibrated and continuous global time-series heritage and pathfinder satellite imagery such as National Oceanic and Atmospheric Administration's (NOAA's) Advanced Very High Resolution Radiometer (AVHRR) and Landsat provide a great opportunity to study land-cover changes over time. The datasets from Smith *et al.* (1997) facilitated the generation of quantitative information on land-use/land-cover change (LULCC) for any place in the World from July 1981 to September 2001: the period for which well calibrated continuous time-series AVHRR pathfinder 10 km (0.1-degree) datasets are available. Such historical information is invaluable in investigations such as drought studies (Thenkabail *et al.*, 2004b), monitoring LULCC, change detection of any type (e.g., changes due to a major irrigation scheme), and hydrological or land-cover modeling. These datasets contain four spectral bands (see Table 1) as a monthly or 10-day synthesis by the National Aeronautics and Space Administration's (NASA) Goddard Space Flight Center (GSFC): **http://daac.gsfc.nasa.gov/data/dataset/AVHRR/01_Data_Products/04_FTP_Products/index.html**. The monthly composite data are superior to 10-day composites in terms of cloud free pixels (Wen and Tateishi, 2001), allowing composition of a continuous series of monthly images as a single mega-file for

P.S. Thenkabail and H. Turral are with the International Water Management Institute Headquarters, P.O. Box 2075, Colombo, Sri Lanka (p.thenkabail@cgiar.org).

P. GangadharaRao, T.W. Biggs, and M. Krishna are with the International Water Management Institute Regional office, Hyderabad, Andhra Pradesh, India.

Photogrammetric Engineering & Remote Sensing
Vol. 73, No. 9, September 2007, pp. 1029–1040.

0099-1112/07/7309–1029/$3.00/0

TABLE 1. THE 956-BAND AVHRR MEGA-FILE CHARACTERISTICS FOR KRISHNA BASIN. A CONTINUOUS STREAM OF MONTHLY 0.1-DEGREE AVHRR DATA FROM 1981 TO 2001 WAS USED IN THE STUDY[1,2]

Band Number[3] (#)	Wavelength Range (μm)	Duration[4] (years)	Number of Bands for 1982 to 2000 (#; one per month)[5]	Data Final Format (percent: for reflectance)[6]	Range[8] (percent)
				(degree Kelvin: temperature) (unitless: for NDVI)[7]	
Band 1 (B1)	0.58–0.68	1982–2000	224	reflectance (at-ground)[9]	0–100
Band 2 (B2)	0.73–1.1	1982–2000	224	reflectance (at-ground)[9]	0–100
Band 4 (B4)	10.3–11.3	1982–2000	224	Brightness temperature (top-of-atmosphere)	160–340
Band 5 (B5)	11.5–12.5	1982–2000	224	Brightness temperature (top-of-atmosphere)	160–340
NDVI[7]	(B2 − B1)/(B2 + B1)	1982–2000	224	unitless	−1 to +1

Notes:
1 = Data were acquired from NOAA satellites 7 (13 July, 1981 through 05 February, 1985), 9 (06 February, 1985 through 07 November, 1988), 11 (08 November, 1988 through 14 September, 1994), and 14 (03 January, 1995 to 31 December, 2000). The 0.1-degree (approximately 10 km) product was generated using global area coverage (GAC) data (4 km × 4 km).
2 = NOAA is a sun synchronous, near polar orbiting satellite at 833 km above earth imaging at at 98.8 degrees, with ascending node local overpass times of 14.30 (NOAA-7), 14.20 (NOAA-9),13.30 (NOAA-11), and13.30 (NOAA-14), orbiting the Globe every 102 minutes (14.1 orbits daily).
3 = Band 3 (3.55 to 3.93 μm) was not used due to unresolved calibration issues.
4 = Data is actually available for 1981 to 2001. But we have used 19 complete years (1982 to 2000) in this study.
5 = There was data for 224 months in 19 years. September to December 1994 data was not acquired due to failure of the satellite.
6 = The reflectance data is corrected for Rayleigh Scattering and ozone absorption (see James and Kalluri, 1994)
7 = pixels with highest NDVI's were chosen in monthly time-compositing, nearly providing cloud-free images.
8 = Data from all bands were converted to surface reflectance using time invariant desert sites from Sahara and Arabia.
9 = At ground reflectance, since the data has gone through corrections for atmospheric scattering and absorption.

the entire globe from 1981 to 2001 (**http://www.iwmidsp.org**). However, the use of satellite sensor data for historical understanding of quantitative change is complicated by the absence of historical ground truth data and/or historical high resolution images that coincide with different AVHRR time series.

The value of historical time-series (HTS) AVHRR data (or for that matter, any similar historical data) will be enhanced several-fold if a rational, automated technique of identifying and labeling classes from the historical data is developed. There are a number of traditional techniques of time-series data analysis that include Fourier harmonic analysis, fast Fourier transformation (FFT), wavelet techniques (e.g., Jakubauskas *et al.*, 2002; Olsson and Eklundh, 1994), principal component analysis, change detection analysis (Jensen, 2000), artificial neural networks, and decision trees (Defries *et al.*, 1998; Mather, 2003). Each of these methods have strengths and limitations. The Fourier sinusoidal components or harmonics depict mono- or bi-modality of the curve from which inferences such as single crop or double crop are derived, and generally can be a powerful approach for irrigated area mapping. But it is generally known that in highly fragmented and mixed cropping scenario Fourier analysis provides noisy trends (Jakubauskas *et al.*, 2002; Olsson and Eklundh, 1994). In general, Fourier provides good results for regular periodic signals. Wavelet analysis is suitable for highly non-stationary signals that possess sudden picks and discontinuities (Jaffard *et al.*, 2001), but is not very sensitive to changes in magnitude of the signal of closely linked classes. It is well known that the principal component analysis (PCA) components that model the largest contributions to the data set variance may work poorly for pattern recognition (Tucker *et al.*, 1986). Change detection techniques are widely used, but it is well known that there are errors associated with each of the two land-cover maps, and when these are overlaid, the errors are cumulative. As a result, the error of the land-cover change map is significantly worse than either of the land-cover maps (see Jensen, 2000). Artificial neural networks (ANN) are hindered by the need to specify values of a number of parameters (Mather, 2003). Decision trees are increasingly popular, computationally easier, and considered superior to other time-series analysis methods such as ANN, change detection, and PCA (see Mather, 2003; DeFries *et al.*, 1998). However, decision trees are difficult to apply for historical time-series for which little or no knowledge exists.

Spectral Matching Techniques (SMT's) (in a following section) are a new innovative method of identifying and labeling information classes in historical time-series (HTS) data. Hitherto, applied in hyperspectral analysis of minerals, the SMTs offer powerful qualitative and quantitative techniques and methods. In time-series analysis of imagery, typically, historical time series (HTS) spectra are "matched" with the "target" spectra of recent time-series (RTS) and/or from ideal endmember classes for which class names are known through existing knowledge base such as census data, ground truth, and maps of the study area. The quantitative and qualitative spectral "matching" of a class continues until the spectral time series of a class from HTS time-period fits with one of the classes of RTS and/or ideal endmember class. Once this is achieved it becomes possible to decipher its class identity and hence label HTS classes.

Thereby, the overarching goal was to establish the qualitative and quantitative spectral matching techniques (SMTs) to identify and label historical time-series land-use/land-cover (HTS-LULC) classes based on "target" spectra. The approaches, methods, and techniques were tested using monthly AVHRR data for HTS time period (1982 to 1985) and RTS time period (1996 to 1999). The 1982 to 1985 time period was considered ideal HTS as it was at the beginning of swift rise in irrigation projects in the basin. From 1996 to 1999, a period in which almost all major irrigation projects were completed, the ground water expansion plateaued. The change in irrigation in particular after 1999 was considered insignificant based on field knowledge.

Methods

Study Area

The method was tested and validated for the Krishna River basin in India, which is one of the benchmark river basins of the International Water Management Institute (IWMI) and for which substantial field data is available for the recent and historical time periods. The Krishna River basin (Figure 1), the third largest river basin in India after the Ganges, Godavari, encompasses a total area of 26,708,800 hectares, about 8 percent of the geographic area of India. The Krishna originates in the Western Ghats and flows east into the Bay of Bengal (Figure 1). The Krishna flows through three states: Karnataka, Maharastra, and Andhra Pradesh (see Figure 1). The average annual rainfall for the basin is about 800 mm, almost all of which falls during the Monsoon months of June through October. The long-term mean rainfall of the delta region is about 900 mm, and that of the Western Ghats is about 2,500 mm, but they occupy less than 25 percent of the basin area. About 75 percent of the Krishna basin has a semi-arid climate, with mean rainfall of about 650 mm. Hence, full or supplementary irrigation is a key to livelihoods in these areas throughout the year. With numerous new irrigation projects developed in the last three decades, the land-use and irrigated areas have changed considerably. Given the above facts, the basin is an ideal location to test spectral matching techniques (SMTs).

Characteristics of AVHRR Data Used in this Study

The AVHRR time-series data for the Krishna river basin was subseted from the calibrated global continuous time-series mega dataset (see **http://www.iwmidsp.org**) composed from the individual files available from NASA GSFC (**www.daac.gsfc.gov/data/dataset/AVHRR**). There were four missing months, September through December 1994 due to a failure of the NOAA AVHRR system. In total there are 239 months of data for each band, making a total of 956 bands from Band 1, 2, 4, and 5 for the entire basin, the characteristics of which are listed in Table 1. Band 3 was not used due to unresolved calibration issues (see Smith *et al.*, 1997).

The monthly composites are generated through the maximum value compositing (MVC) technique of the daily AVHRR data (Smith *et al.*, 1997). The MVC technique selects the data on the date with the maximum NDVI of a given pixel over the month. The procedure involves quality checks (Goward *et al.*, 1994; Eidenshink and Faundeer, 1994) and normalization for sun-angle (Cihlar *et al.*, 1994) needed as a result of different orbital paths and acquisition time of various NOAA satellites. Aerosol has significant influence on visible and NIR bands, and its effects are known to remain uncorrected, even after long compositing periods (e.g., a month) (Vermote *et al.*, 2002). Many factors lead to variations or shifts in the data, including but not limited to, sensor degradation, change in sensor design, satellite orbital characteristics, atmospheric effects, topographic effects, moisture absorption effects, and sun illumination. These effects have been addressed through several stages of calibrations and re-calibrations (e.g., Smith *et al.*, 1997; Rao, 1993a and 1993b; Kidwell, 1991; Gordon *et al.*, 1988; Fleig *et al.*, 1983; NGDC, 1993), making AVHRR a high quality science dataset. For the thermal channels, first the atmosphere radiances was calculated and converted to brightness temperatures using a Planck function equivalent lookup table based on the response curve of each channel (Smith *et al.*, 1997). The data used in this study, was further calibrated by choosing "perfect" sites in the Libyan Sahara desert (see Rao, 1993a and 1993b) and Saudi Arabian desert that are "time-invariant" over time. The data were then normalized by developing calibration coefficient and/or calibration factor. These methods take a long-time mean of these time invariant locations and correct individual images to long-term mean. A full discussion is beyond the scope of this paper, but the 20-year mega-file data and calibrations are made available through **http://www.iwmidsp.org.**

The original 16-bit (0 to 65536 digital number) scaled-reflectance data downloaded from NASA GSFC are converted to four calculated variables, using the conversion coefficients provided in the accompanying documentation, that transforms data to reflectance (0 to 100 percent) for band 1 and band 2 and brightness temperature (degrees Kelvin) for band 4 and 5. The four calculated variables are: (a) at-ground reflectance, (b) top of atmosphere brightness temperature, (c) surface temperature, and (d) NDVI. These parameters were derived using calibration parameters in the following six equations (see Smith *et al.*, 1997):

$$\text{Reflectance (percent)} = (\text{Band 1 scaled DN in 16-bit radiance} - 10) * 0.002 \quad (1)$$

$$\text{Reflectance (percent)} = (\text{Band 1 scaled DN in 16-bit radiance} - 10) * 0.002 \quad (2)$$

$$\text{Normalized difference vegetation index (NDVI) (unit less)} = (\text{SNDVI} - 128) * 0.008 \quad (3)$$

$$\text{Band 4 brightness temperature (degrees Kelvin)} = (\text{Band 4 scaled DN in 16-bit} + 31990) * 0.005 \quad (4)$$

$$\text{Band 5 brightness temperature (degrees Kelvin)} = (\text{Band 5 scaled DN in 16-bit} + 31990) * 0.005 \quad (5)$$

Surface temperature (Ts) is calculated using split window technique, assuming a constant emissivity of 0.96.

$$\text{Surface temperature } (Ts) = T_4 + 3.3\,(T_4 - T_5) \quad (6)$$

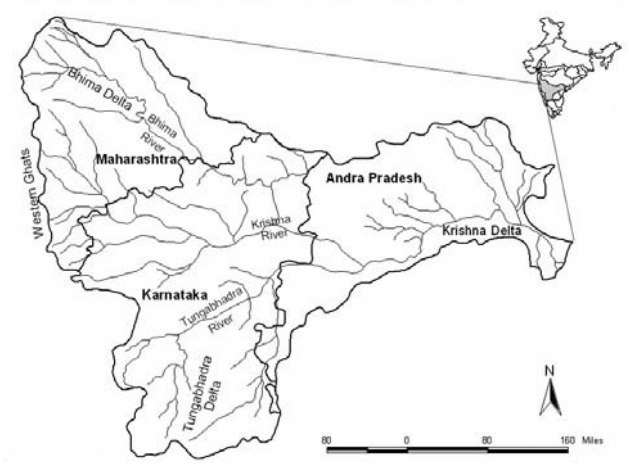

Figure 1. Location map of Krishna river basin, India. The basin is spread across three Indian states: Andhra Pradesh, Karnataka, and Maharastra.

Characteristics of Ground-truth Data Used in this Study

Ground-truth (GT) data was collected for the recent time-series (RTS) during 13–26 October 2003 for 144 sample sites covering about 6,500 kilometers of road travel in the

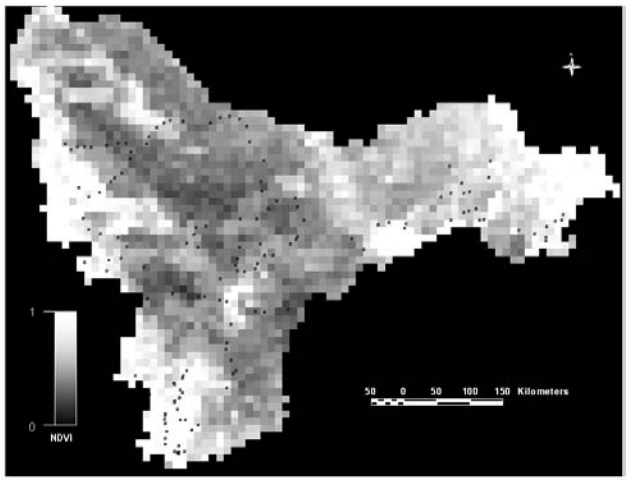

Figure 2. Ground-truth (GT) data point locations. The GT data from 144 locations consisted of land-use, land-cover, cropping pattern, crop types, and watering method (e.g., rainfed, irrigated).

Krishna River basin (Figure 2). Much of the changes in the basin occurred during 1980 to 1995 when most irrigation projects were completed and operationalized. The LULC and irrigated area changes from RTS (1996 to 1999) and GT data collection period (2003) was minimal as established through: (a) survey of India land-use maps for year 2000 for certain parts of the basin, and (b) knowledge base from various researchers working in the basin. In addition, ground truth observations were made extensively, while driving, by digitizing on hard-copy topographic maps (1:500 000) obtained from the Survey of India. The Geocover 2000 (Tucker *et al.*, 2004; **http://glcf.umias.umd.edu/index.shtml**) products were also used as additional ground-truth information in class identification.

Point specific data was collected from 90 m by 90 m plots and consisted of GPS locations, land-use categories, land-cover percentages, cropping patterns during different seasons (through farmer interviews), crop types, and watering method (irrigated, rainfed). Samples were obtained within large contiguous areas of a particular land-use/land-cover (LULC). A stratified-systematic sample design was adopted. The framework was stratified by motorable road network or foot path access, where possible, made systematic by locating sites every 5 or 10 kilometers along the road network by vehicle or on foot (see Thenkabail *et al.*, 2005 and Thenkabail *et al.*, 2004a for a detailed description on the ground truth methodological approaches). The real challenge is to collect data from the 90 m by 90 m sample location to represent 10 km by 10 km area. We accomplished this by first selecting a "representative" location for each class. The representativeness was established through a reconnaissance of AVHRR 10 km class through spatial contiguity of class as determined through higher resolution Landsat ETM+ data and MODIS 500 m time-series data.

Spectral Signature Matching (SSM) to Determine Historical LULC

Spectral signature matching (**SSM**) techniques are traditionally developed for hyperspectral data analysis of minerals (e.g., Homayouni and Roux, 2003; Shippert, 2001, Bing *et al.*, 1998; Farrand and Harsanyi, 1997; Granahan and Sweet, 2001; Thenkabail *et al.*, 2004 c and 2004d). Time-series data, such as the monthly NDVI data from AVHRR, are similar to hyperspectral data tens or hundreds of months in time-series data replacing tens or hundreds of bands in hyperspectral data. These similarities imply that the spectral matching techniques (SMTs), applied for hyperspectral image analysis, also have potential for application in identifying historical land-use/land-cover (HTS-LULC) classes from historical time-series satellite imagery. This involves qualitative and quantitative spectral matching of the HTS-LULC classes with the target spectra which is either ideal spectra of endmembers and/or recent time-series LULC (RTS-LULC) classes. The RTS-LULC classes are first identified and labeled using the recent ground-truth field data and recent high-resolution Landsat TM imagery: then HTS-LULC classes are identified by "matching" HTS class spectra to RTS-LULC class spectra and/or ideal endmember class spectra through SMTs to identify and label HTS-LULC classes. The quantitative and qualitative SSM methods are described below.

Quantitative Spectral Matching Techniques (SMTs)

Spectral Correlation Similarity (SCS): Shape Measure

The spectral correlation similarity (SCS), between the time-series NDVI spectral profile of HTS-LULC classes ($NDVIH_i$) and the time-series NDVI spectral profile of RTS-LULC classes ($NDVIR_i$), provides one indication of spectral similarity. The assumption is that the spectral profile of similar LULC classes such as irrigated agriculture of historical time-series (HTS) and irrigated agriculture of the recent time series (RTS), will have greater correlation coefficients (SCS R^2 values) than unrelated (or dissimilar) classes, such as irrigated agriculture of HTS and rainfed agriculture or any other class of RTS. The SCS or R^2 values or ρ (referred to as SCS R^2 values or simply SCS) are computed as follows (SAS, 2004; van der Meer and Bakker, 1997):

$$SCS = \frac{1}{n-1}\left[\frac{\sum_{i=1}^{n}(t_i - \mu_t)(h_i - \mu_h)}{\sigma_t \sigma_h}\right] \quad (1)$$

where, t_i = target (a RTS-LULC class or a ideal LULC class) spectra or NDVI @ time $i = 1$ to n, μ_t = mean spectra or NDVI of target, h_i = historical (a HTS-LULC class) spectra or NDVI @ time $i = 1$ to n, μ_h = mean spectra or NDVI of historical class, σ_t = standard deviation of target class spectra or NDVI, and σ_h = standard deviation of historical class spectra or NDVI.

The "SCS or R^2 values or ρ" (SCS R^2 values or simply SCS) values, typically, vary between 0 and 1, and primarily measure the shape of the spectra over time.

Interpretation of SCS = A shape measure: The higher the SCS, the greater the similarity in the shape of spectral or temporal NDVI profile between the HTS-LULC classes and RTS-LULC classes. An r value of 0 is least similar, 1 most similar (ideal).

Euclidian Distance Similarity (EDS): distance measure

The Euclidian distance (or Spectral Distance) measures determine the closeness or separation between a HTS-LULC class and the RTS-LULC classes in spectral space (Campbell, 1987):

$$EDS = \sqrt{\sum_{i=1}^{n}(t_i - \rho_i)^2} \quad (2)$$

where t, ρ, and n are defined in Equation 1. The above formula is normalized to 0 to 1, by using historical minimum (m) and historical maximum (M) NDVI of the target class as shown below:

$$EDSnormal = (Ed_{orig} - m)/(M - m). \quad (3)$$

EDSnormal (Closeness and/or separability) is between 0 and 1, and primarily measures the magnitude of NDVI closeness or separability over time. $E_{d\ orig}$ = Euclidian distance at the origin.

Interpretation for *EDSnormal* = A Distance Measure: The distance or proximity between spectra or temporal NDVI of HTS-LULC classes with RTS-LULC classes. Zero is most separate, 1 most close.

Spectral Similarity Value (SSV): Shape and Distance Measure
The SSV combines the characteristics of SCS and SDS. It combines measures of shape (correlation) and NDVI difference (closeness) between HTS-LULC classes and RTS-LULC and/or ideal endmember spectral classes (Homayouni and Roux, 2003; Granahan and Sweet, 2001):

$$SSV = \sqrt{EDS^2 + (1 - \rho)^2} \tag{4}$$

The range of the SSV is between 0 to 1.414.

Interpretation for SSV = A Shape and Distance Measure: Similarities of: (a) distance, and (b) shape between spectra or temporal NDVI of HTS-LULC classes with RTS-LULC classes. The smaller the SSV values, the greater the similarity between the spectra and vice versa.

Modified Spectral Angle Similarity (MSAS)
The spectral angle between the HTS-LULC NDVI ($NDVI_H$) of a class at given time to recent RTS-LULC NDVI ($NDVI_R$) of a class at given time is first established. Then, the hyper-angle (angle between target spectrum and pixel spectrum) is defined as an angle between $NDVI_H$ versus $NDVI_R$ of all classes at every date. The hyper-angle is defined as (Shippert, 2001; Homayouni and Roux, 2003; Farrand and Harsanyi, 1997; Schwarz and Staenz, 2001):

$$\alpha = across\left[\frac{\sum_{i=1}^{n} t_i pi}{\sqrt{\sum_{i=1}^{n} t_i^2}\sqrt{\sum_{i=1}^{n} p_i^2}}\right] \tag{5}$$

$$MSASnormal = \frac{2\alpha}{\pi}. \tag{6}$$

The range of $MSAS_{normal}$ is between 0 to 1. The interpretation for $MSAS_{normal}$ is the hyper-angle between spectra or temporal NDVI of HLULC classes with RLULC classes. Smaller the hyper-angle (or smaller the $MSAS_{normal}$) greater the similarity between the spectra and vice versa.

Qualitative SSM Approaches

A qualitative SSM approach takes the time-series spectra of one HTS-LULC and matches it for shape and magnitude with all RTS-LULC classes and/or ideal spectral classes (often for simplicity only RTS-LULC is mentioned). The HTS-LULC class being matched is assigned to one of the RTS-LULC classes based on: (a) shape, and/or (b) magnitude, and/or (c) both shape and magnitude. The categorization and labeling adhere to the following protocol:

1. If the shape and magnitude of the HTS-LULC class match with one of the RTS-LULC class, then its (HTS-LULC) class ID is assigned to that RTS-LULC class; and
2. If the HTS-LULC class has only shape or magnitude match with one of the RTS-LULC class, then its (HTS-LULC) class ID is only partially established to be the same as the RTS-LULC class with which it has shape or magnitude matches.

The qualitative measures are used in conjunction with the quantitative measures. When certain trends are seen in qualitative measures, they are verified through quantitative measures. When there is conclusive evidence from qualitative measures, quantitative measures help strengthen the inference. When there is absence of conclusive evidence from qualitative measures, quantitative measures are solely depended on.

Results and Discussion

First, the results and discussion on RTS-LULC (1996 to 1999) are presented. The RTS-LULC classes are determined using normal unsupervised classification backed by bispectral plots, NDVI plots, detailed ground truth, and census statistics. This will be followed by results and discussion on HTS-LULC classes using innovative spectral matching techniques (SMTs). First, qualitative SMTs will be presented and discussed, followed by quantitative and spatial. Specific emphasis will be on irrigated area class for which ground-truth (GT) data is also richer. Finally, accuracy assessment of the irrigated area class in the HTS-LULC classes will be established.

The RTS-LULC

The RTS-LULC classes were derived from AVHRR monthly time series of 1996 to 1999. The original AVHRR continuous time-series mega-file data for 1981 to 1999 consisted 956 bands. Of this, the RTS data for 1996 to 1999 consisted of 192 bands (4 bands * 4 years * 12 months). Initially, statistical algorithm called "ISOCLASS" for unsupervised clustering was performed on the RTS 192 band dataset using ERDAS Imagine® 8.7. The monthly AVHRR NDVI images for 1996 to 1999 were used to capture the RTS-LULC characteristics. Classifications such as these, using multiple years, capture climate variability (wettest to driest years) and is a better representation of actual LULC and irrigated area conditions for a period (e.g., late-1990s) than using a single month or a single year.

The mean 1996 to 1999 month-by-month long-term mean thermal "skin" temperature (Figure 3a) and AVHRR NDVI (Figure 3b) and are presented for the initial 19 classes

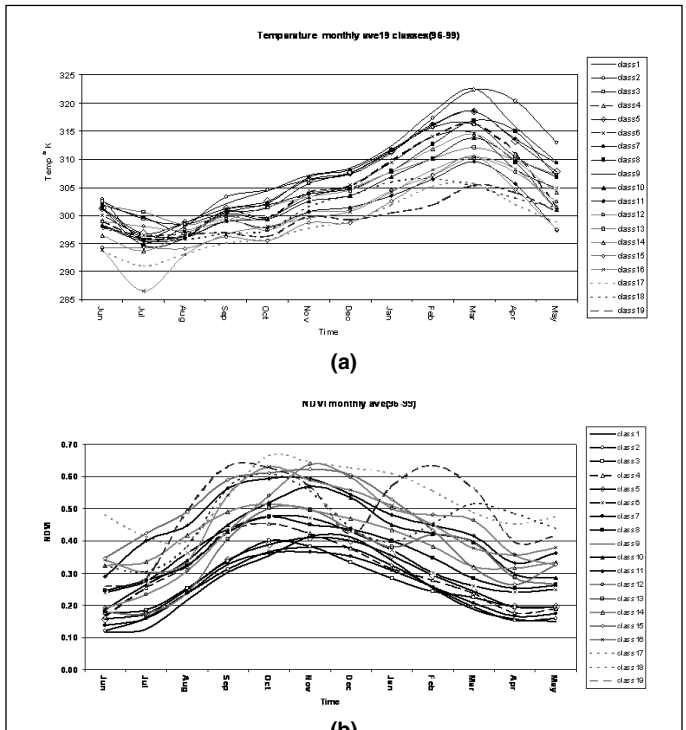

Figure 3. The NDVI and "skin" temperature profiles for identifying and labeling RTS (1996 to 1999) LULC classes. The mean monthly "skin" temperature (b) and NDVI (a) and profiles of the 19 RTS-LULC classes were used in distinguishing classes based on their difference over time.

of the RTS-LULC. All classes follow a pattern based on seasonality; a steep rise in NDVI at the beginning June to July of main cropping season called "Khariff," high NDVI during peak-Kariff (August to October), moderate and decreasing NDVI during beginning of second cropping season called "Rabi" (November to February), and low NDVI during summer (March to June) (see Figure 3b). The results highlight a strong degree of relationships between AVHRR NDVI and rainfall (see Eklundh, 1998) and their significant relationships with biophysical quantities (Foody *et al.*, 1983). The "skin" temperature (Figure 3a) is almost perfectly opposite to the NDVI (Figure 3b) behavior; when NDVI is high, "skin" temperature is low and vice versa. All 19 classes follow a consistent pattern, with classes being separated from one another based on the magnitude of variation (Figure 3a and 3b). The availability of thermal images, in addition to red and NIR, enhances class seperability further, supporting the results of Kerber and Schutt (1986), Lumbin and Ehrlich (1995 and 1996), and Maxwell *et al.* (2002a and 2002b). Thermal skin temperature, T_s, responds to variations in the energy balance caused by evapotranspiration from the land surface, which may be affected by both short term processes such as surface wetting by rainfall, and longer term, seasonal processes, such as changes in soil moisture, vegetation cover, and cropping pattern (Wen and Tateishi, 2001; Lambin and Ehrlich, 1995). The ratio between Ts and NDVI increases the capability of discrimination among vegetation classes (Goward *et al.*, 1991 and 1994; Huete and Liu, 1994; Jensen, 2000; Kogan and Zhu, 2001; Lambin and Ehrlich, 1995). The ratio of Ts/NDVI has been interpreted biophysically as regional surface resistance to evapotranspiration (Nemani and Running, 1989).

The classes were identified and labeled on the basis of the ground-truth data, including field observations and interviews, NDVI and temperature profiles (e.g., Figure 3a and 3b), brightness-greenness-wetness (BGW) plots (e.g., Figure 4a through 4d) (see Thenkabail *et al.*, 2005 for methods and approaches of using BGW plots), and space-time spiral-curves (ST-SCs; Thenkabail *et al.*, 2005) (Figure 5). Two-dimensional feature space (2D-FS) plots are illustrated for all 19 RTS-LULC classes using Band 1 (red) and Band 2 (NIR) (Figure 4). These 2D-FS BGW plots are illustrated for selected months of peak winter (or Rabi) crop, peak summer (May), peak vegetative during monsoon (August), and critical phases during monsoon (October) (see Figure 4a through Figure 4d). The classes were significantly closer to the soil line during the driest periods (Figure 4b) compared to the monsoonal periods (Figure 4c and 4d). The BGW plots are also plotted for peak-Khariff (monsoonal season) month of October (Figure 4d) and peak-Rabi (winter) month of January (Figure 4a). The classes are significantly closer to the soil line during summer (Figure 4b) and winter (Figure 4a) relative to monsoonal periods (Figure 4c and 4d) as a result of higher biomass and vegetation cover during Khariff. The classes moved around in space and time significantly. For example, take classes 14, 8, and 2 that were close to each other in February (Figure 4a). The classes 14 and 2 were significantly different in October (Figure 4d) than the classes 14 and 8 in August (Figure 4c). Overall, almost all the classes can be distinguished from other classes in one season or the other. The brightness, greenness, and wetness (BGW) zones (Crist and Cicone, 1984) capture unique land-cover classes and help us separate them into distinct categories. Tree canopies and hills have deeper shadows compared with crops. The BGW zones (Figure 4a through 4d) help us capture this phenomenon very well. Within a class such as agricultural crops, ST-SCs (Figure 5) separate irrigated rice, irrigated mixed crops and rainfed crops. The ST-SCs (Figure 5) are a powerful 3D (*x, y*, and time as third dimension) graphical approach to studying subtle and not-so-subtle variation in biomass dynamics over time for each class and are illustrated for the forest, irrigated, and rainfed classes in Figure 5. These three classes, for example, occupy unique domains in 3D feature space for dry years (Figure 5). There are one or more dates in which all three classes are spectrally well separated (Figure 5). The forests are in the green-wet zone, irrigated in the green zone, and rainfed in the bright-green zone. These series of plots, backed by ground truth data, and census statistics lead to a final seven aggregated RTS-LULC classes (Figure 6a).

The heterogeneity within the 10 km pixels can cause difficulty in identifying a particular pixel with a particular class. Thereby, the final seven RTS-LULC and irrigated area classes (see Figure 6a) were identified from the original 19 classes based on actual ground truth data, field interviews, Survey of India maps, spectral BGW plots (e.g., Figure 4), ST-SCs (e.g., Figure 5), NDVI time-series plots (e.g., Figure 3a), and "skin" temperature (e.g., Figure 3b) time-series plots.

The HTS-LULC (1982 to 1985) and the Spectral Matching Techniques (SMTs)

The HTS classes could not be directly labeled because of the complete absence of ground-truth data for 1982 to 1985, so the spectral matching techniques (SMTs) were adopted to identify classes.

The initial 21 unsupervised classes (not illustrated) were narrowed down to seven final HTS-LULC classes (Figure 6b) based on:

1. Qualitative spectral matching;
2. Quantitative spectral matching; and
3. Spatial location of the class as pseudo-ground information.

Combinations of the above methods (Hill and Donald, 2003; Wang *et al.*, 2001; Granahan and Sweet, 2001) play a key role in accurate matching of classes and labeling them. It needs to be noted that the quantitative, qualitative, and spatial SMT's are complementary/supplementary in how they are used. This means that we can use them interchangeably to resolve, identify, and label classes. The RTS-, and the HTS-LULC classes were all labeled to match each other (e.g., class 1 in HTS is the same as class 1 in RTS, or class 5 in HTS is the same as class 5 in RTS, and so on) based on the methods and approaches previously discussed. When a class "matches" in characteristics in one time-period relative to the other, it was assigned a unique code.

The Qualitative Spectral Signature Matching (SSM) Techniques for HTS-LULC

The HTS-LULC classes were first identified by a qualitative spectral matching technique (SMTs) that involved using the "target" spectra from: (a) RTS-LULC classes, and (b) ideal endmember class locations. The spectra of each of the original 21 spectral classes of HTS were matched with the seven available RTS-LULC and irrigated area class spectra (see, for example, Figure 7a through 7d). The process of matching is carried out until a combination of HTS classes constitutes a "spectral match" in shape and/or magnitude with the RTS classes (see Figure 7). Ground-truth classes were extensively used to determine how we match classes. So, classes were matched not only based on how well they spectrally match, but that have meaningful grouping based on field knowledge. The shape of the RTS classes matched the HTS classes well (Figure 7a through 7d), but the magnitudes of the classes, however, were sharply higher for RTS-LULC, compared to HTS spectral profiles. The irrigated areas (Figure 7d), for example, have intensified with technological improvements, (increased cropping intensities, and intensive crop management practices) all of which resulted in a sharp rise of biomass levels during the RTS, in comparison to the

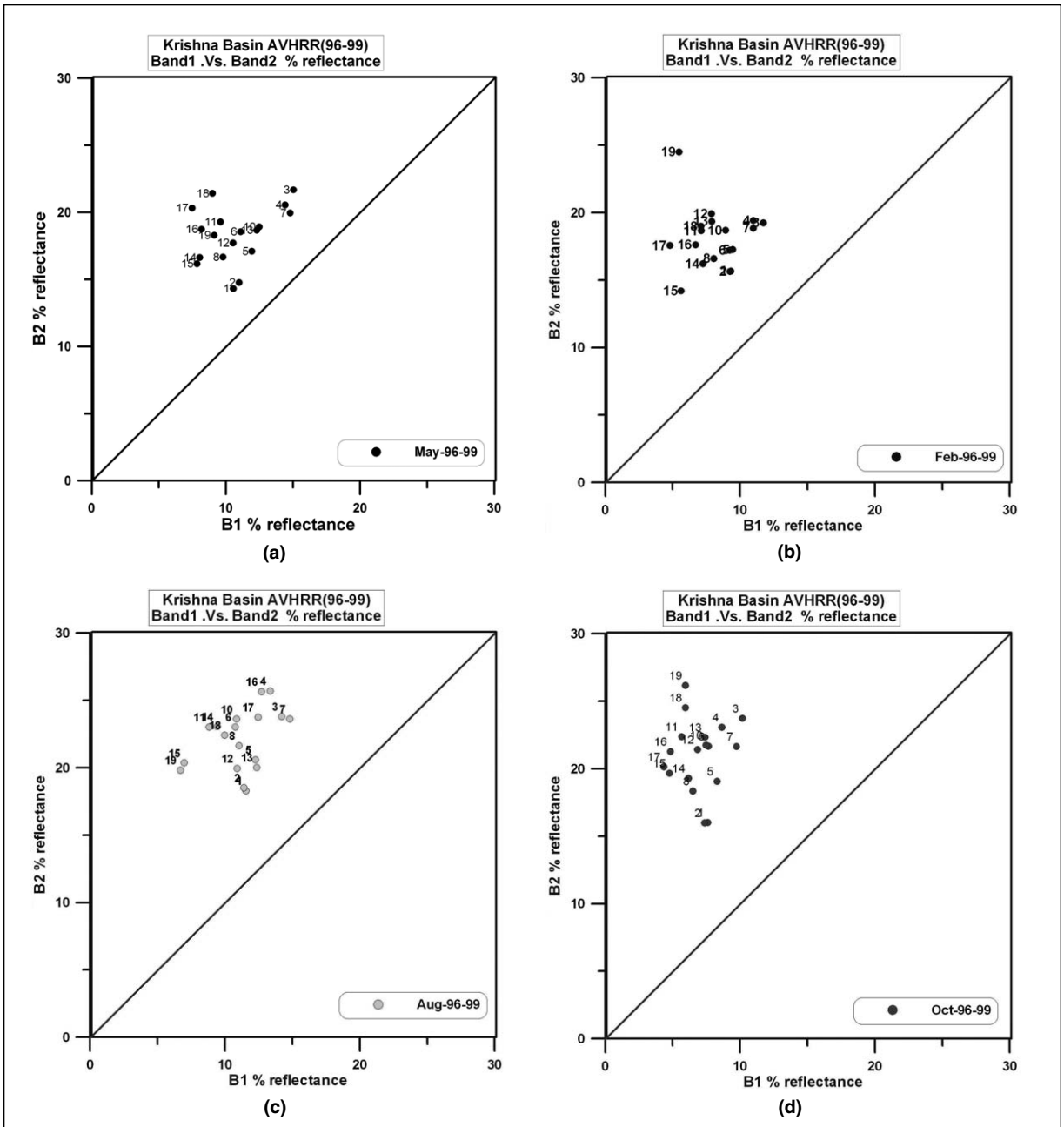

Figure 4. The brightness-greenness-wetness (BGW) 2-dimensional feature space (2D-FS) plots for identifying and labeling RTS (1996 to 1999) LULC classes. The BGW 2D-FS plots of AVHRR band 1 versus band 2 reflectivity for the 19 RTS LULC classes are illustrated for average monthly conditions for 1996 to 1999 RTS period for the months of: (a) February (peak winter crop), (b) May (peak summer), (c) August (mid-monsoonal rainy season), and (d) October (peak monsoonal rainy season).

HTS. The spectral matches of HTS with RTS-LULC are also illustrated for irrigated (supplemental) class 4 (Figure 7c), pure rainfed class 3 (Figure 7b), and dryland agriculture class 1 (Figure 7a). Again, the shape itself matches well with an offset in magnitude (Shippert, 2001; Staenz and Williams, 2001a; Schwarz and Staenz, 2001b).

There are two significant noticeable changes in the HTS spectra relative to RTS spectra. First, the magnitudes of spectra (e.g., NDVI) of the RTS classes were significantly higher than the magnitude of the spectra of the HTS classes (see, for example, Figure 7c and 7d). Second, the shape of the NDVI spectra were more "U" shaped for the RTS classes, compared to the more "V" shaped for the HTS classes (Figure 7a, 7b, and 7c). The "U" shapes indicate greater intensity of cropping or vegetation over longer periods. The "V" shapes are more for single cropping. The magnitude of the changes is as a result of technological advances (e.g., crop management practices, fertilizer, and greater cropping intensity) and/or physical infrastructure changes (e.g., installation of groundwater wells, irrigation infrastructure, and related greater efficiency and reliability in water delivery). For example, the biomass and grain yield have increased consistently over last two decades of the millennium and now has reached plateau. This was established

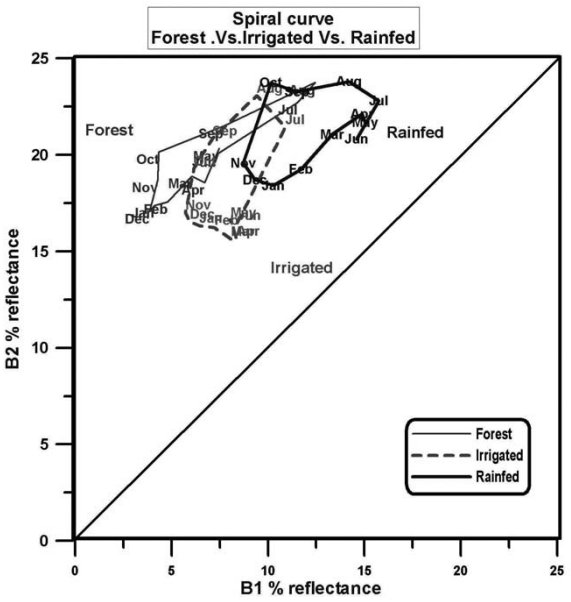

Figure 5. Space-time spiral-curves (ST SCs) for identifying and labeling the 19 RTS (1996 to 99) LULC classes. The reflectivity in band 1 (red) versus band 2 (NIR) plotted continuously for each month from June 1998 to May 1999 and illustrated for three classes: forests (class 7) versus irrigated (class 5) versus rainfed agriculture (class 3). The ST-SCs are in away 3D plots (*X,Y*, and time) and show the time (in months) during which two classes can be differentiated.

based on interviews of farmers, local agricultural extension officers, and researchers working in the area. This is true even for rainfed agriculture. Further, there has been swift increase in ground water irrigation, often to supplement rainfed agriculture. All these factors have increased biomass levels of all agricultural crops irrigated and non-irrigated alike.

Quantitative Indices for HTS-LULC Identification and Labeling

The indices previously introduced were used to quantify class similarity as a quantitative check on the qualitative matching used to assign historical class names. The qualitative matching was used first, since the quantitative matching tended to merge classes that had different land-cover based on ground truth data.

The matrix of spectral correlation similarity (SCS) R^2 values for time-series HTS-LULC NDVI versus RTS-LULC NDVI are shown in Table 2. Five of the seven classes of HTS-LULC had the highest SCS R^2 values for their corresponding RTS-LULC classes determined by using the qualitative spectral matching approach (Table 2). For example, class 2 of HTS-LULC has an SCS R^2 value of 0.97 with class 2 of RTS-LULC, whereas the R^2 values with all other classes were substantially lower. The R^2 measure accounts for shape of the spectra, and so would account for differences in the timing of vegetation phenologic transitions, but not total vegetation cover or irrigation intensity.

The SSV (Table 3) measures both the shape and the magnitude of the NDVI spectra. Six of the seven classes of HTS and the "target" had the lowest SSV values or greatest spectral similarity (Table 3). The "target" spectra were obtained from the RTS-LULC and/or ideal locations of the seven classes. For example, the irrigated area class 5 for

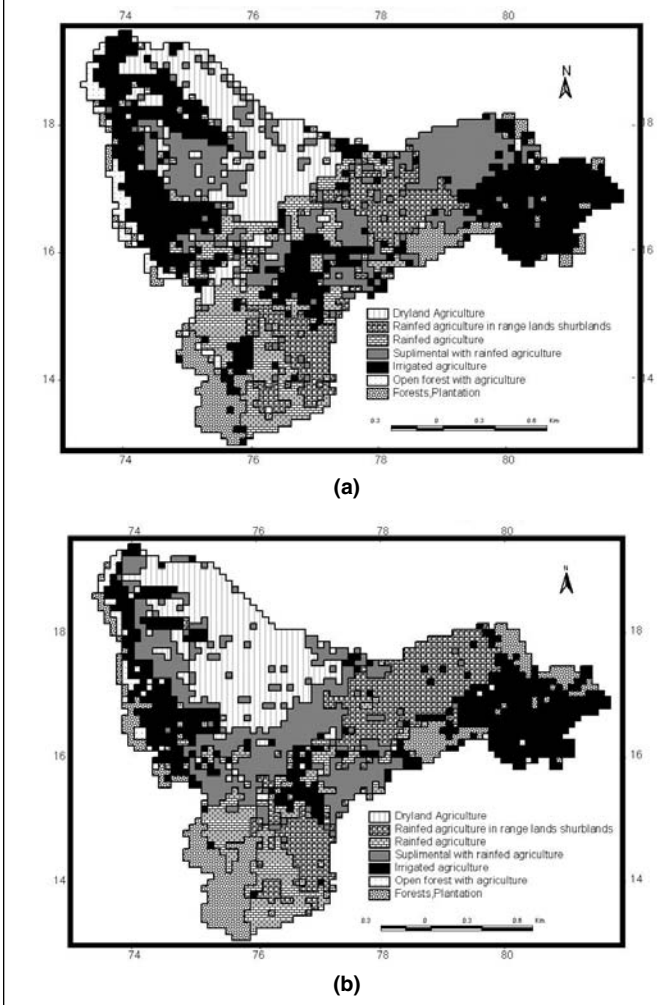

Figure 6. The final seven RTS- and HTS-LULC class maps of Krishna basin. The spatial distribution of the final seven classes using the AVHRR 0.1-degree monthly data was mapped for the: (a) 1996 to 1999 RTS-LULC, and (b) 1982 to 1985 HTS-LULC.

1982 through 85 had the lowest SSV value (or greatest similarity) of 0.22 with the class 5 (irrigated) spectra of the ideal target for the class.

The results of E_d were similar to the results obtained from SCS R^2 values and the modified spectral angle similarity (MSAS) (see Homayouni and Roux, 2003) provided similar results as SSV. Hence, it was not necessary to report these. Further, the MSAS is more complex to compute, and has a tendency to provide "infinity." Given these facts, it is obvious that computation of SSV would suffice. The supplemental irrigated class 4 of HTS was hardest to determine using RTS data (see, for example, Table 3) as a result of dramatic changes of conversion of other classes in HTS to supplemental irrigated class in RTS. Also, in RTS the magnitude of NDVI increased as a result of the intensity and technological advances in crop growth conditions. The final spectral characteristics of the RTS-LULC and HTS-LULC are depicted in Figure 8a and 8b. The final spatial distribution of RTS-LULC and HTS-LULC are shown in Figure 6a and 6b, respectively. The area under each class and changes in area of the seven classes are shown in Table 4 and will be discussed in a section to follow.

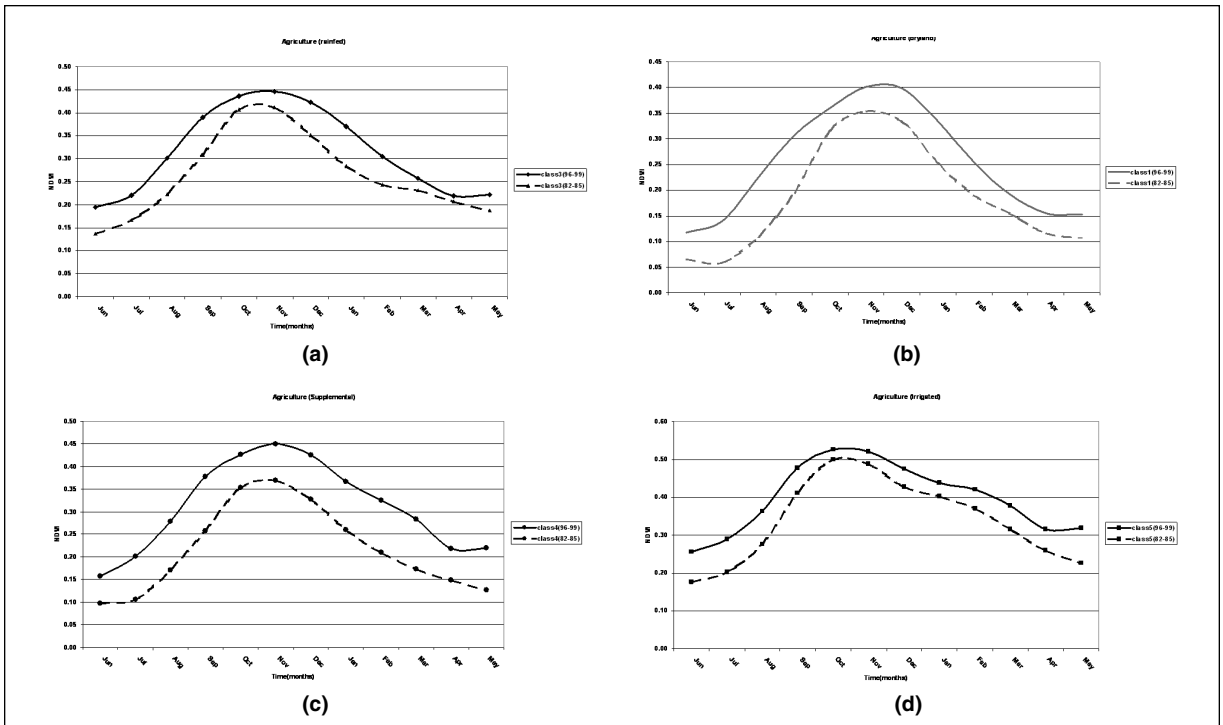

Figure 7. Qualitative spectral matching techniques. Illustration of qualitative spectral matching technique between RTS-LULC classes and HTS-LULC classes for: (a) dryland agriculture, (b) rainfed agriculture, (c) supplemental irrigated agriculture, and (d) irrigated agriculture.

TABLE 2. SPECTRAL CORRELATION SIMILARITY (SCS) VALUE. THE SCS VALUES FOR SEVEN CLASSES DURING 1982 TO 1985 VERSUS 1995 TO 1999. THE SCS WERE ESTABLISHED BASED ON THE CORRELATION (R^2 VALUE) MATRIX BETWEEN MONTHLY TEMPORAL SPECTRAL NDVI PROFILES OF 1982 TO 1985 VERSUS 1995 TO 1999

	Class 1-9599	Class 2-9599	Class 3-9599	Class 4-9599	Class 5-9599	Class 6-9599	Class 7-9599
Class 1-8285	**0.93**	0.73	0.88	0.92	0.87	0.89	0.88
Class 2-8285	0.82	**0.97**	0.90	0.86	0.88	0.77	0.79
Class 3-8285	0.90	0.89	0.93	**0.94**	***0.94***	0.90	0.85
Class 4-8285	0.96	0.87	0.96	**0.96**	0.94	0.92	0.91
Class 5-8285	0.91	0.85	0.92	0.97	**0.98**	0.91	0.86
Class 6-8285	0.79	0.72	0.80	0.85	0.88	**0.95**	0.82
Class 7-8285	0.82	0.74	0.82	0.83	0.83	***0.94***	0.88

Note: SCS values vary between 0 to 1. Greater the SCS, greater the spectral similarity.

TABLE 3. SPECTRAL SIMILARITY VALUE (SSV). THE SSV VALUES FOR SEVEN CLASSES DURING 1982 TO 1985 VERSUS IDEAL TARGET SPECTRA FOR THE SAME PERIOD

	Class 1-target	Class 2-target	Class 3-target	Class 4-target	Class 5-target	Class 6-target	Class 7-target
Class 1-8285	**0.23**	0.33	0.19	0.43	0.30	0.39	0.35
Class 2-8285	0.23	**0.15**	0.17	0.39	0.29	0.48	0.43
Class 3-8285	0.28	0.18	**0.17**	0.45	0.25	0.44	0.35
Class 4-8285	0.25	0.15	**0.16**	0.57	0.27	0.48	0.39
Class 5-8285	0.36	0.28	0.24	0.29	**0.22**	0.33	0.26
Class 6-8285	0.35	0.29	0.29	0.22	0.23	**0.20**	0.29
Class 7-8285	0.46	0.34	0.34	0.17	0.43	0.15	**0.15**

Note: SSV values vary between 0 to 1.414. Lesser the SSV value greater the spectral similarity.

Spatial Matching in HTS-LULC Identification and Labeling

Care must be taken when interpreting SCS R^2 values and the SSV values as it is very likely, but not necessarily true, that a HTS class belongs to the same RTS-LULC class with which it has highest SCS and SSV values. There are situations when two spectra with matching SCS and SSV values have quite different vegetation cover and cropping intensities, like continuous irrigation, forest, and agro-forest. Therefore, a "blind" assignment of classes, based just on quantitative highest correlations alone should be avoided. In other words, a quantitative match must be corroborated by evidence from field knowledge, interviews, and multiple checks.

In Table 2, the best SCS values for class 3 (rainfed agriculture) of HTS-LULC is with class 5 (irrigated agriculture) or Class 4 (Supplemental and rainfed agriculture) of RTS-LULC,

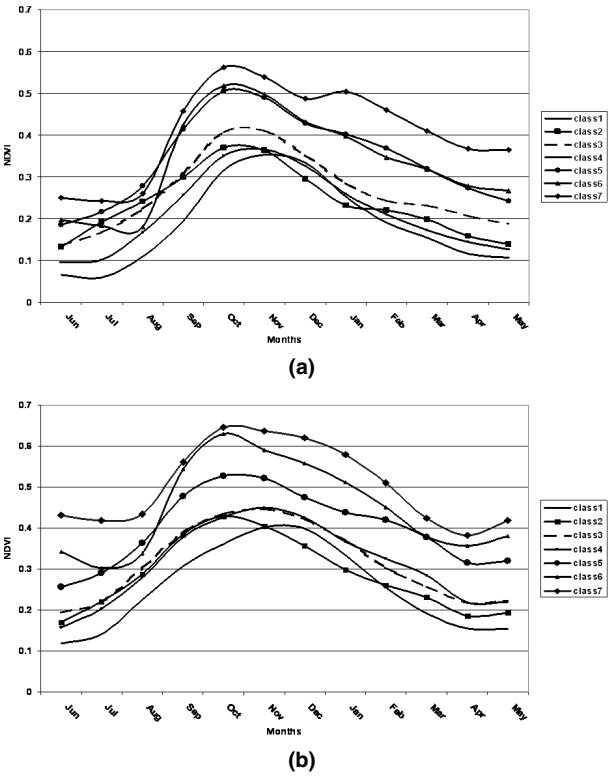

Figure 8. **The final seven RTS- and HTS-LULC class characteristics.** The final seven class characteristics as depicted using NDVI plots for the: (a) 1996 to 1999 RTS-LULC, and (b) 1982 to 1985 HTS-LULC.

TABLE 4. HISTORICAL LAND-USE/LAND-COVER CHANGE (LULCC) IN KRISHNA BASIN. THE LULCC IN KRISHNA BASIN STUDIES USING AVHRR 0.1-DEGREE DATA FOR TIME PERIODS: (a) 1981 TO 2001 CONTINUOUS MONTHLY STREAMS, (b) HISTORICAL 1982 TO 1985 MONTHLY, AND (c) RECENT 1995 TO 1999 MONTHLY

For the Time Periods Historical Time Series (82–85), Recent Time Series (96–99)				
Class#	Class Description	82–85 %	96–99 %	Difference 96–99 to 82–85 %
Class1	Agriculture (dryland)	18.07	14.24	−3.84
Class2	Rangelands	16.03	10.65	−5.39
Class3	Agriculture (rainfed)	10.36	15.14	4.77
Class4	Agriculture (Supplemental)	18.97	19.87	0.90
Class5	Agriculture (Irrigated)	22.85	30.03	7.18
Class6	Forests (degraded) with agriculture mosaic	1.96	2.73	0.78
Class7	Forests, plantations	11.75	7.34	−4.41

Note:
A = total area of the basin = 267,088 sq. kms.
1 = when compared with 1982 to 1985, in 1996 to 1999 significant portion of the class 1 (dryland) and class 2 (rangelands) are converted into class 3 (rainfed) and class 4 (supplemental);
2 = when compared with 1982 to 1985, in 1996 to 1999 significant portion of the class 4 (supplemental) is converted into class 5 (irrigated).
3 = when compared with 1982 to 1985, in 1996 to 1999 significant portion of the class 7 (Forests, plantations) is converted into class 6 (Forests degraded with agriculture).

and not with class 3 (rainfed agriculture) of RTS (Table 2). This is because the characteristics of rainfed agriculture in RTS (1995 to 1999) changed, when compared with HTS (1982 to 1985) (Figure 7). The agricultural classes: dryland (Figure 7a), rainfed (Figure 7b), and supplemental (Figure 7c) all had "inverted U shape" NDVI time-series in RTS period when compared with "inverted V shape" NDVI time-series in HTS period. The U shape implies greater length of cropping period compared to V shape. The rainfed agriculture season now stretches from July of one year to March of next year in RTS, giving NDVI time-series spectra a "inverted U shape," whereas rainfed crop was mainly grown during August to February during HTS and had a "inverted V shape" (Figure 7b). Field visits indicated that this is as a result of increased groundwater irrigation or increased intensity and frequency of rainfed cropping in a calendar year in RTS compared to HTS. Therefore, going purely by quantitative SCS and SSV values as in Table 2 or Table 3 or by qualitative observations as in Figure 7, without paying attention to spatial location of class could be, at times, misleading. Thereby, once the qualitative and quantitative relationships are established, further confirmation of the class matches were confirmed based on spatial location of the occurrence of the class. For example, the best SCS values for class 5 (Irrigated agriculture) of HTS is with class 5 (irrigated agriculture) of RTS (Table 2). Class 5 of RTS has a similar shape to class 5 of HTS, except that there was greater vigor and hence, higher NDVIs during RTS (Figure 7d). So both were labeled class 5 based, not only on quantitative (Table 2) and qualitative (Figure 7b) observations of time series NDVI spectra, but were verified further by spatial location of their occurrences (Figures 6a and 6b). There are times when, for example, continuous irrigation (e.g., sugarcane) may show up similar to forests in qualitative and quantitative HTS and RTS spectra, but the spatial location of forests are distinct compared to sugarcane agricultural areas.

Accuracy of Irrigated Areas from Historical Data

The accuracies of mapping irrigated areas were assessed using data from field based maps made available by basin administration (CBIP, 1984), results from two other studies (one using National irrigation statistics and another remote sensing approaches), and by adopting sub-pixel (see Biggs *et al.*, 2006) and full-pixel area calculations. The sub-pixel irrigated areas (SPIAs) of the Krishna basin determined in this study for 1996 to 1999 are compared with two other SPIA estimates: (a) FAO/Frankfurt University irrigated area (Siebert *et al.*, 2002), and (b) IWMI Global Irrigated Area Map (Thenkabail *et al.*, 2005b). The Frankfurt University map used mid-1990s statistics from the National statistics on irrigated areas and created a global map of irrigated areas providing the irrigated percent of the area/pixel. The IWMI global irrigated area map used 0.1-degree AVHRR data of 1997 to 1999 (same as this study) along with other datasets, such as GTOP30, rainfall, SPOT vegetation 1 km, and forest cover data to determine spatial location of irrigated areas, and then used sub-pixel decomposition (SPD) technique to obtain irrigated areas. These calculations showed the area irrigated in the Krishna basin was 3,589,500 hectares (93 percent of our estimate) from the Frankfurt map, and 3,415,600 hectares (88.5 percent of our estimate) from the IWMI global map.

For the HTS time period (1982 to 1985), the irrigated areas mapped in this study were compared with the irrigated areas of 1984 provided by the Central Board of Irrigation and Power of India (CBIP, 1984). The CBIP produced a comprehensive map of irrigated areas for all India from which the Krishna basin statistics were extracted. The total irrigated during 1982 to 1985 as determined in this study for the Krishna basin was 2,975,800 hectares, which is 108.47 percent of the CBIP (2,743,368 hectares) estimate. These results clearly proved the utility of AVHRR historical time series in determining irrigated areas (and by corollary, other LULC classes) from the past, adding great value to time-series data.

Conclusions

This paper proposed and demonstrated the use of spectral matching techniques (SMTs) in determining historical LULC and irrigated areas (HTS-LULC) classes using the historical time series 0.1-degree AVHRR data for which little or no ground truth data is available.

Two quantitative spectral matching techniques were found most useful: First, spectral similarity value (SSV) which measures the shape as well as the magnitude similarities of the time series spectra. This was followed by spectral correlation similarity (SCS) which measures only the shape of the time series spectra. The other methods like Euclidian distance and modified spectral angle similarity were more complex, provided uncertain results, and did not at any time provide better results than SSV and SCS. Qualitative methods are used in conjunction with quantitative methods to strengthen the inferences drawn from each other. Quantitative methods are primary, qualitative measures supportive. The implementation protocols of using these techniques were well established and described in the paper. Currently, there is proliferation of time-series satellite sensor data from sensors such as MODIS Terra and Aqua and in the future advanced sensor systems such as National Polar Operational Environmental Satellite System (NOPESS). The SMTs are ideal in analyzing time-series satellite sensor data, especially adding value to historical images. A major application of SMTs will be to "match" class spectra with ideal spectra for myriad applications such as crop type identification, plant species identification, and mineral exploration. The SMT methods can be further strengthened by additional research involving these subject areas by using rich ground based knowledge base.

References

Biggs, T.W., P.S. Thenkabail, M.K. Gumma, M. Krishna, C. Scott, P. GangadharaRao, and H. Turral, 2006. Vegetation phenology and irrigated area mapping using combined MODIS time-series, ground surveys, and agricultural census data in Krishna River Basin, India, *International Journal of Remote Sensing*, 27(19):4245–4266.

Bing, Z., L. Jiangu, W. Xiangjun, and W. Changshan,, 1998. Study on the classification of hyperspectral data in urban area, *SPIE*, Vol. 3502.0277-786x/98.

Boas, M.L., 1983. *Mathematical Methods in the Physical Sciences*, Second Edition, New York, John Wiley & Sons, pp. 648–652.

Brady, N.C., and P.R. Weil, 2002. *The Nature and Properties of Soils*, Upper Saddle River, Prentice Hall, pp. 206–210.

Campbell, J.B., 1987. *Introduction to Remote Sensing*, The Guilford Press, New York, 551 p.

CBIP, 1984. *Irrigation Map of India 198*4, Central Board of Irrigation and Power (CBIP), Malcha Marg, Chanakyapuri, New Delhi-110021.

Cihlar, J., D. Manak, and M.D'Iorio, 1994. Evaluation of compositing algorithms for AVHRR data over land, *IEEE Transactions on Geosciences and Remote Sensing*, 32:427–437.

Cihlar, J., H. Ly, and Q. Xiao, 1996. Land cover classification in AVHRR multichannel composites in Northern Environments, *Remote Sensing of Environment*, 58:36–51.

Congalton, R.G., and K. Green, 1999. *Assessing the Accuracy of Remotely Sensed Data: Principles and Practices*, New York, Lewis Publishers.

Crist, E.P., and R.C. Cicone, 1984. Application of the Tasseled Cap concept to simulated Thematic Mapper data, *Photogrammetric Engineering & Remote Sensing*, 50(3)343–352.

DeFries, R., M. Hansen, and J. Townshend, 1995. Global discrimination of land cover types from metrics derived from AVHRR Pathfinder data, *Remote Sensing of Environment*, 54, 209–222.

DeFries, R., M. Hansen, J.G.R. Townsend, and R. Sohlberg, 1998. Global land cover classifications at 8 km resolution: The use of training data derived from Landsat imagery in decision tree classifiers, *International Journal of Remote Sensing*, 19:3141–3168.

Dymond, C.C., D.J. Mladenoff, and V.C. Radeloff, 2002. Phenological differences in Tasseled Cap indices improve deciduous forest classification, *Remote Sensing of Environment*, 80:460–472.

Eidenshink, J.C., and J.L. Faundeen, 1994. The 1 km AVHRR global land data set: First stages in implementation, *International Journal of Remote Sensing*, 15(17):3443–3462.

Eklundh, 1998. Estimating relations between AVHRR NDVI and rainfall in East Africa at 10-day and monthly time scales, *International Journal of Remote Sensing*, 19 (3):563–568.

Farrand W.H., and J.C. Harsanyi, 1997. Mapping the distribution of mine tailings in the Coeur d'Alene River Valley, Idaho, through the use of a constrained energy minimization technique, *Remote Sensing of Environment*, 59:64–76.

Fleig, A.J., D.F. Heath, K.F. Klenk, N. Oslik, K.D. Lee, H. Park, P.K. Bartia, and D. Gordon, 1983. *User's Guide for the Solar Backscattered Ultraviolet (SBUV) and the Total Ozone Mapping Spectrometer (TOMS) RUT-S and RUT-T Data Sets: October 31, 1978 to November 1980*, NASA Reference Publication 1112.

Foody, G.M., D.S. Boyd, and P.J. Curran, 1996. Relations between tropical forest biophysical properties and data acquired in AVHRR channels 1–5, *International Journal of Remote Sensing*, 17, 1341–1355.

Gopal, S., C. Woodcock, and A.H. Strahler, 1996. Fuzzy ARTMAP classification of global land cover from AVHRR data set, *Proceedings of the 1996 International Geoscience and Remote Sensing Symposium*, Lincoln, Nebraska, 27–31 May, pp. 538–540.

Goodchild, M.F., 1988. The issue of accuracy in global databases, *Building Databases for Global Science* (H. Mounsey, editor), New York, Taylor and Francis, pp. 31–48.

Goward, S.N., B. Markham, D.G. Dye, W. Dulaney, and J. Yang, 1991. Normalized difference vegetation index measurement from the Advanced Very High Resolution Radiometer, *Remote Sensing of Environment*, 35:257–277.

Goward, D.G., S. Turner, D.G. Dye, and J. Liang, 1994. University of Maryland improved Global Vegetation Index, *International Journal of Remote Sensing*, 15(17):3365–3395.

Granahan, J.C., and J.N. Sweet, 2001. An evaluation of atmospheric correction techniques using the spectral similarity scale, *Proceedings of the IEEE 2001 International Geoscience and Remote Sensing Symposium*, Vol. 5, pp. 2022–2024.

Jaffard, S., Y. Meyer, and R.D. Ryan, 2001. *Wavelets: Tools for Science & Technology*, Society for Industrial and Applied Mathematics, Philadelphia, 256 p.

Jakubauskas, M.E., D.R. Legates, and J.H. Kastens, 2002. Crop identification using harmonic analysis of time-series AVHRR NDVI data, *Computers and Electronics in Agriculture*, 37(1–3):127–139.

Harsanyi, J.C., 1993. *Detection and Classification of Subpixel Spectral Signatures in Hyperspectral Image Sequences*, Ph.D. Dissertation, University of Maryland, Baltimore County.

Hill, M.J., and G.E. Donald, 2003. Estimating spatio-temporal patterns of agricultural productivity in fragmented landscapes using AVHRR NDVI time series, *Remote Sensing of Environment*, 84:367–384

Homayouni, S., and M. Roux, 2003. Material mapping from hyperspectral images using spectral matching in urban area, *Submitted to IEEE Workshop in Honour of Professor Landgrebe*, Washington D.C.

Huete, A.R., and H.Q. Liu, 1994. An error and sensitivity analysis of the atmospheric-correcting and soil-correcting variants of the NDVI for the MODIS-EOS, *IEEE Transactions on Geoscience and Remote Sensing*, 32(4):897–905.

Jensen, J.R., 2000. *Remote Sensing of the Environment: An Earth Resource Perspective*, Prentice Hall, New Jersey, pp. 333–373.

Kerber, A.G., and J.B. Schutt, 1986. Utility of AVHRR channel 3 and 4 in land-cover mapping, *Photogrammetric Engineering & Remote Sensing*, 52(12):1877–1883.

Kidwell, K., 1991. *NOAA Polar Orbiter Data User's Guide*, NCDC/SDSD, National Climatic Data Center, Washington, D.C.

Kogan, F.N., and X. Zhu, 2001. Evolution of long-term errors in NDVI time series: 1985–1999, *Advances in Space Research*, 28(1):149–153.

Lambin, E.F., and D. Ehrlich, 1995. Combining vegetation indices and surface temperature for land-cover mapping at broad spatial scales, *International Journal of Remote Sensing*, 16:573–579.

Lambin, E.F., and D. Ehrlich, 1996. The surface temperature-vegetation index space for land-cover and land-cover change analysis, *International Journal of Remote Sensing*, 17:1–15.

Maxwell, S.K., R.M. Hoffer, and P.L. Chapman, 2002a. AVHRR channel selection for land cover classification, *International Journal of Remote Sensing*, 23(23):5061–5073.

Maxwell, S.K., R.M. Hoffer, and P.L. Chapman, 2002b. AVHRR composite period selection for land cover classification, *International Journal of Remote Sensing*, 23(23):5043–5059.

NGDC, 1993. *5 Minute Gridded World Elevation*, NGDC Data Announcement DA 93-MGG-01, Boulder, Colorado.

Olsson, L., and L. Eklundh, 1994. Fourier-series for analysis of temporal sequences of satellite sensor imagery, *International Journal of Remote Sensing*, 15(18):3735–3741.

Rao, C.R.N., 1993a. Nonlinearity corrections for the thermal infrared channels of the Advanced Very High Resolution Radiometer: Assessment and recommendations, *NOAA Technical Report NESDIS-69. NOAA/NESDIS*, Washington, D.C.

Rao, C.R.N., 1993b. Degradation of the visible and near-infrared channels of the Advanced Very High Resolution Radiometer on the NOAAP9 spacecraft: Assessment and recommendations for corrections, *NOAA Technical Report NESDIS-70, NOAA/NESDIS*, Washington, D.C.

Schwarz, J., and K. Staenz, 2001. Adaptive threshold for spectral matching of hyperspectral data, *Canadian Journal of Remote Sensing*, 27(3):216–224.

Shippert, P., 2001. Spectral and hyperspectral analysis with ENVI, *ENVI User's Group Notes*, 22–28 April, Annual meeting of the American Society of Photogrammetry and Remote Sensing, St. Louis, Missouri.

Siebert, S., P. Döll, and J. Hoogeveen, 2002. *Global Map of Irrigated Areas*, Version 2.1, Center for Environmental Systems Research, University of Kassel, Germany and FAO, Rome, Italy, URL: http://www.geo.unifrankfurt.de/ipg/ag/dl/forschung/Global_Irrigation_Map/index.html (last date accessed: 05 June 2007).

Smith, P.M., S.N.V. Kalluri, S.D. Prince, and R.S. DeFries, 1997. The NOAA/NASA Pathfinder AVHRR 8-km land data set, *Photogrammetric Engineering & Remote Sensing*, 63(1):12–31.

Staenz, K., and D. Williams, 1997. Retrieval of surface reflectance from hyperspectral data using a look-up table approach, *Canadian Journal of Remote Sensing*, 23(4):354–368

Thenkabail, P.S., C.M. Biradar, H. Turral, and M. Schull, 2005a. *A Global Map of Irrigated Area at the End of the last Millennium using Multi-sensor, Time-series Satellite Sensor Data*, Documentation on Global Map of Irrigated Area, International Water Management Institute, pp. 77, URL: http://www.iwmigmia.org (last date accessed: 05 June 2007).

Thenkabail, P.S., M. Schull, and H. Turral, 2005b. Ganges and Indus River Basin land Use/Land cover (LULC) and irrigated area mapping using continuous streams of MODIS data, *Remote Sensing of Environment*, 95(3):317–341.

Thenkabail, P.S., N. Stucky, B.W. Griscom, M.S. Ashton, J. Diels, B. Van Der Meer, and E. Enclona, 2004a. Biomass estimations and carbon stock calculations in the oil palm plantations of African derived savannas using IKONOS data, *International Journal of Remote Sensing*, 25(23):5447–5472.

Thenkabail, P.S., N. Gamage, and V. Smakhin, 2004b. The use of remote sensing data for drought assessment and monitoring in southwest Asia, *IWMI Research Report # 85*, IWMI, Colombo, Sri Lanka, pp. 25.

Thenkabail, P.S., E.A. Enclona, M.S. Ashton, C. Legg, and M. Jean De Dieu, 2004c. Hyperion, IKONOS, ALI, and ETM+ sensors in the study of African rainforests, *Remote Sensing of Environment*, 90:23–43.

Thenkabail, P.S., E.A. Enclona, M.S. Ashton, and V. Van Der Meer, 2004d. Accuracy assessments of hyperspectral waveband performance for vegetation analysis applications, *Remote Sensing of Environment*, 91(2–3):354–376.

Tucker, C.J., C.O. Justice, and S.D. Prince, 1986. Monitoring the grasslands of the Sahel: 1984–1985, *International Journal of Remote Sensing*, 7:1571–1582.

Tucker, C.J., D.M. Grant, and J.D. Dyktra, 2004. NASA's Global orthorectified Landsat data set, *Photogrammetric Engineering and Remote Sensing*, 70(3):313–322.

van der Meer, F., and W. Bakker, 1997. CCSM: Cross correlogram spectral matching, *International Journal of Remote Sensing*, 18:1197–1201.

Wang, J, K.P. Price, and P.M. Rich, 2001. Spatial patterns of NDVI in response to precipitation and temperature in the central Great Plains, *International Journal of Remote Sensing*, 22: 3827–3844.

Wen, C.G., and R. Tateishi, 2001. 30-second degree grid land cover classification of Asia, *International Journal of Remote Sensing*, 22(18):3845–3854.

(Received 12 December 2005; accepted 10 January 2006; revised 15 March 2006)